



# A numerical and experimental study through laser thermography for defect detection on metal additive manufactured parts

N. Montinaro, D. Cerniglia, G. Pitarresi

Dipartimento dell'Innovazione Industriale e Digitale (DIID), Università degli Studi di Palermo, Palermo, Italy  
nicola.montinaro@unipa.it; <https://orcid.org/0000-0001-9607-3324>



**ABSTRACT.** Additive manufacturing has been recently employed in industrial sectors with the fundamental requirement for zero defect parts.

Technological developments in additive manufacturing notwithstanding, there continues to be a scarcity of non-destructive inspection techniques to be exploited during the manufacturing process itself, thus limiting industrial advancements and extensive applications.

Therefore, being able to integrate the defect inspection phase within the additive manufacturing process would open the way to enabling corrective actions on the component *in itinere*, that is, before reaching the final product. For this reason, new methods of in-process monitoring are gaining more and more attention nowadays.

In this work, a remote laser thermographic methodology is employed as a mean to detect micrometric defects in additive manufactured samples. Beforehand, a preliminary Finite Element Analysis was carried out in order to optimize the sensitivity of the technique to the micrometric defects. Our results indicate that the technique is proved to be quite successful in detecting flaws, with the added plus of being suitable for integration in the additive manufacturing equipment, thus allowing a continuous in-line inspection.

**KEYWORDS.** Non-destructive testing; IR Thermography; Additive Manufacturing, Laser Thermography, FEA, Modeling.

**Citation:** Montinaro, N., Cerniglia, D., Pitarresi, G., A numerical and experimental study through laser thermography for defect detection on metal additive manufactured parts, *Frattura ed Integrità Strutturale*, 43 (2018) 231-240.

**Received:** 12.11.2017

**Accepted:** 10.12.2017

**Published:** 01.01.2018

**Copyright:** © 2018 This is an open access article under the terms of the CC-BY 4.0, which permits unrestricted use, distribution, and reproduction in any medium, provided the original author and source are credited.

## INTRODUCTION

Recently, additive manufacturing (AM) has been getting more and more attention in the areas of 3D geometries production and high-value parts repair, due to its increased accuracy in creating complex structures as compared to other, more traditional, manufacturing methods. A further benefit is how the mechanical properties of AM components may sometimes even surpass those of conventionally processed parts, as shown in [1]. However, due to the fact that structures are created by superimposing layer after layer, interlayer and intralayer defects can be often observed in AM components, as seen in [2] by means of scanning electron microscopy and microcomputed tomography.



Nonetheless, additive manufacturing has shown great potential in many manufacturing sector, especially in automotive, aerospace, military and medical ones. On one hand, the market scenario for AM parts is constantly growing due to ever new, improved technologies, application areas width and customization possibilities. On the other hand, there remain some drawbacks limiting this market, such as material characterization during development, process and integrity control. In-line inspection would be particularly important in those sectors where verification of AM parts has proven challenging up to now. Indeed, pre-existing non-destructive techniques (NDT) are unable to adapt to the complicated geometries usually created by additive manufacturing. Right now, the soundness of AM parts is evaluated by destructive testing or by X-ray computed tomography (CT) [3], which can only be employed after the part completion, causing parts to be rejected at the end of manufacturing process.

When critical requirements of quality are involved, with the additional complication of dealing with complex geometries, the best option remains a non-destructive technique to be integrated as in-line inspection allowing for the detection of defects as each layer is added. Finally, a non-destructive technique should also be able to detect micrometric flaws, which are a typical occurrence in AM products.

There is previous literature regarding some NDTs used in AM parts. The use of an ultrasonic squirter probe with a standard industrial robot to inspect a 3D metal deposition structure is demonstrated in [4]. Laser-generated surface waves have been used in [5] to investigate laser powder deposition parts, in both stainless steel and titanium, with pores that are simulated using blind holes. Clark et al. in [6] have shown the potential of an all-optical scanning acoustic microscope instrument for online inspection of AM products.

The use of ultrasonic laser transmitter and receiver and the interaction of the incident wave with sub-surface and surface defects have been widely investigated for many different applications [7-10].

A recently introduced NDT active thermographic technique is the flying laser spot technique, which has been employed for the surface crack sizing with micrometric aperture. Li et al. in [11] have developed a thermographic imaging technique using the second spatial derivative of acquired flying laser spot and line thermograms, with the aim of characterizing micrometer cracks in metal samples. In [12] the laser spot imaging thermography was employed and, simultaneously, laser-based ultrasonic measurements to unearth surface breaking cracks. Montinaro et al. in [13] have successfully implemented the flying laser spot technique for the detection and characterization of disbonds and delaminations in fiber metal laminates. The authors monitor the thermal footprint left by the moving heat source, revealing thermal anomalies in a region of interest by using statistical means. The aim of this work is to optimize the parameters used to post-process experimentally acquired thermograms in order to enhance defect sensitivity to micrometric near-surface and surface flaws of additive manufactured parts. The thermal behavior of the sample is thus simulated by a Finite element analysis (FEA) through a transient analysis. The outcomes of the analyses will be used to optimize the experimental procedure. Two Inconel 600 samples with micrometric laser drilled defects have been used as reference for the thermographic experiments. Results from the experiments and the numerical model have been compared showing a sound agreement.

## MATERIALS AND METHODS

### *Flying Laser Inner-Probing Thermography (FLIPT)*

**F**lying Laser Scanning in IR-NDT is characterized by employing a collimated laser heat source that is moved over an object surface. The resulting thermal field is then analyzed to identify and characterize surface or near-surface vertical cracks which behave as barriers towards in-plane heat diffusion [11, 14, 15].

The proposed FLIPT technique uses a laser spot moving at a constant speed, and generating a peculiar temperature profile surrounding the heat source. If the material is uniform and sound, this trailing temperature profile remains unmodified under steady state conditions (i.e. constant laser speed). When the heat source crosses an area over a sub-superficial flaw, the surface temperature field is somewhat disturbed, due to the defective zones stopping temporarily the heat flowing in the through the thickness direction. The defect signature is found in the evolution of the Mean (MT) or the Standard Deviation (SD) of the temperature distribution over a region of interest (ROI) placed on the trail of the heat source. The ROI maintains its position with respect to the laser spot, i.e. it travels at the same speed of the heat source. In [13] the authors have successfully applied the technique for the detection of delaminations on a particular kind of hybrid composite materials called fibre metal laminates.

Fig. 1 shows the set-up used in this work for the laser thermography experiments; Tab. 1 indicates the parameters of the experimental set-up. The sample is installed on a motorized linear micro-slide controlled by PC. The Continuous Wave (CW) laser beam with 1 W of power and 532 nm of wavelength is focused into a 0.75 mm spot on faces A and B of sample 1 and into 0.5 mm on face C of sample 2 (see Fig. 3). The IR camera (see specifications in Tab. 2) is placed perpendicularly



to the sample in order to reduce geometric distortions. It is worth mentioning that the IR camera selected for this application uses a high thermal resolution cooled detector.

The evolution of the generated thermal footprint, while moving the sample at constant speed, is analyzed in the full-filled thermograms acquired with the IR camera. In particular, a sub-window region called ROI is monitored and evaluated offline in the post-processing phase. The ROI is placed in the zone with high temperature gradients behind the heat source, at a certain distance from it. The size of the ROI used in the experimental activity was obtained after the optimization process performed with the numerical model. The scanned surfaces had been preliminary coated with a matt black paint to enhance and uniform the emissivity of radiant energy.

Fig. 2 shows the typical defect signature obtained from the temperature profile acquired with the laser thermography analysis. The local bumps occur when the laser flies over a defected zone. As discussed in [13] the detection mechanism in the flying laser inner probe technique (FLIPT) is based on the perturbation of the heat conduction perpendicularly to the scan direction.

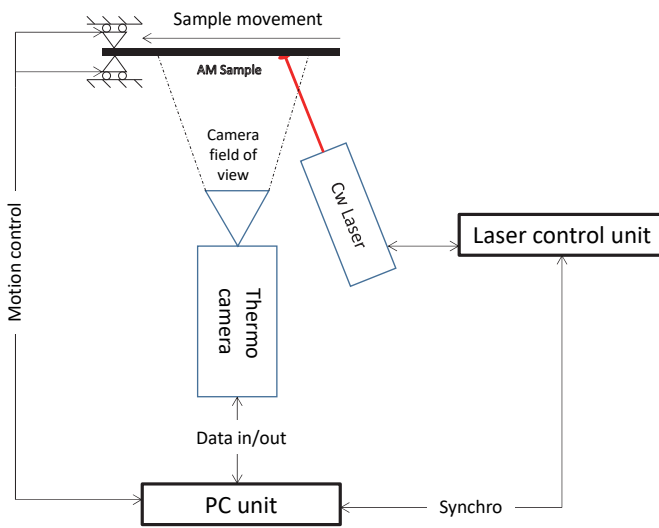


Figure 1: Schematic representation of the experimental setup.

Parameter set-up	Value
Distance sample to IR camera	~300 mm
Distance laser to sample surface	~200 mm
Sample rate IR camera	50 Hz
Laser spot on sample surface	~0.5-0.75 mm

Table 1: Main experimental set-up parameters.

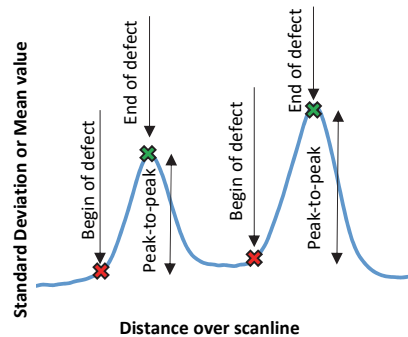


Figure 2: Example of the perturbation on the Standard Deviation or Mean values of the temperature in the ROI when approaching a defect along the scanline.

### The samples

Two reference samples in Inconel 600 have been used with artificial flaws. Laser drilling was used to create holes in the samples, with different diameters ( $\phi$ ) and depths ( $d$ ) below the surface. The two samples geometries are shown in Fig. 3. Sample 1 is a plate with holes below the thickness on faces A and B (see Fig. 3a), drilled at different distances from the edge; sample 2 has a raised portion, representing the first deposited layer above the substrate, where holes were drilled (see Fig. 3b). After laser drilling, dimensions and depths of the holes were measured. It is observed that the laser drilling implemented in this work determines a variation in diameter along the hole drilling depth (see Tab. 3 for an indication of initial and final diameters of the drilled hole defects). Flaw sizes are also reported in Tab. 3.

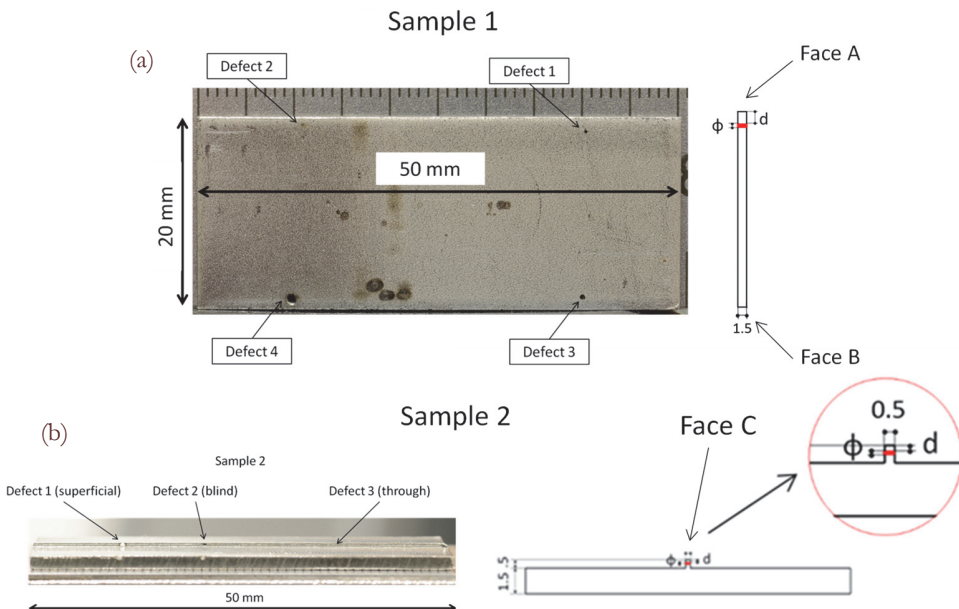


Figure 3: The two geometries of Inconel 600 samples: sample 1 with 4 through holes (a) and sample 2 with 3 holes, among which one superficial and one blind (b).

Thermocamera	
Brand	FLIR
Model	X6540sc
Sensor	Focal Plane array, InSb
Resolution (h×v)	640×512 pixels
Spectral response	1.5–5 $\mu$ m
Lens (hfov × vfov)	MW 25 mm F/2.0 (21.74°×17.46°)
Thermal Resolution (NETD)	20 mK

Table 2: Specification of the IR camera.

Defect/sample	$\phi$ Diameter back/front side (Mean) [ $\mu$ m]	$d$ Depth [mm]	
1/1	700/250 (470)	1.3	Sample 1
2/1	660/190 (420)	0.6	
3/1	800/490 (640)	0.88	
4/1	440/850 (640)	0.9	
1/2	(490)	0	Sample 2
2/2	blind/360	0.1	
3/2	70/330 (200)	0.3	

Table 3: Dimensions and depths of laser drilling holes.



### The Finite Element Model

The thermal behavior of the sample is simulated by a Finite element model through a transient analysis. To avoid convergence issues, an unconditionally stable implicit integration method was used to solve the heat transfer equations. The used heat transfer finite element model was previously compared with analytical and experimental results in [16].

The model of sample 2 was meshed using 105000 4-node linear tetrahedron elements in order to fit the defect geometry without issues. The continuous wave laser source is simulated by considering a focused laser spot as a circular heat source having diameter of 0.5 mm and power of 1 W, fully absorbed by the sample (black body behavior). The thermal behavior of the hole defects is considered as if they were made of air. The natural heat convection at the sample faces is modelled by adopting a surface film condition with sink temperature of 293 K ( $\sim 20^\circ\text{C}$ ).

The FEA provides the distribution of temperature over the whole sample volume for different positions of the heat source, which is supposed to move along a straight line at constant speed. Fig. 4a shows the meshed model of sample 2 while Fig. 4b the lateral view where defects are visible. The element dimensions decrease approaching the zone with the maximum temperature gradient (near the heat source). The heat source is moved at a speed of 5 mm/sec. The thermal properties of the Inconel 600 and of air are: specific heat 444 and 1000 J/kg K and thermal conductivity 14.8 and 0.026 W/m K respectively.

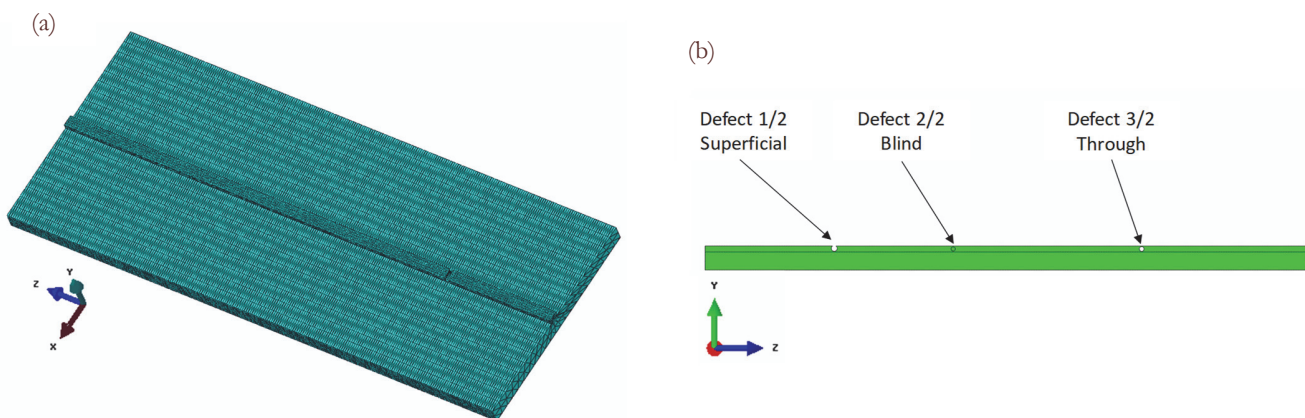


Figure 4: Finite element model of the sample 2: in (a) the meshed sample; in (b) the lateral view of the model with the three defects.

### NUMERICAL RESULTS

**F**ig. 5 shows the temperature map of the modeled sample 2 with the typical trail left by the heat source. In particular maps of the front view (Fig. 5a) and of the transversal  $x$ - $y$  section over the heat source deposition (Fig. 5b) are shown.

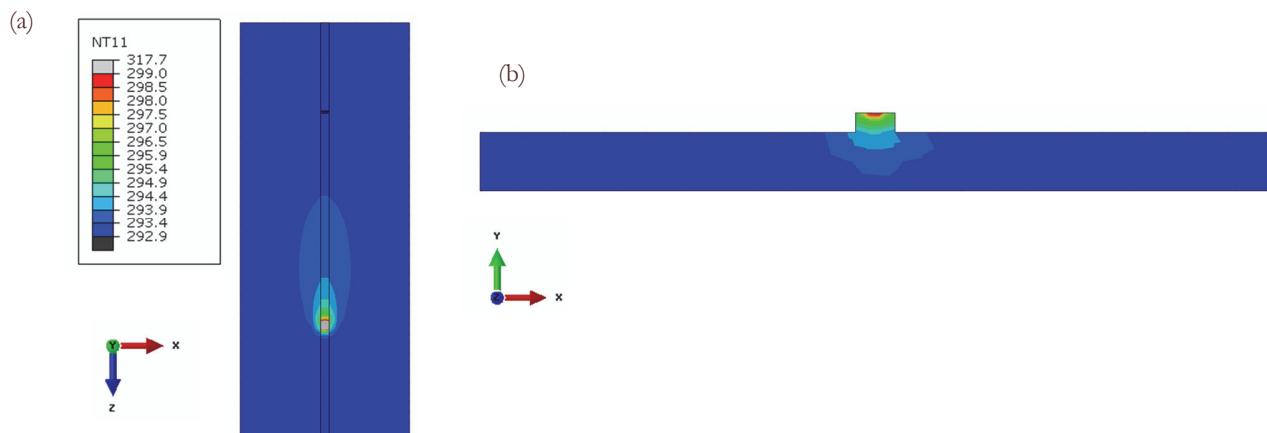


Figure 5: Temperature map of the sample 2: front view (a) and  $x$ - $y$  section view (b); temperature scale in Kelvin degree.

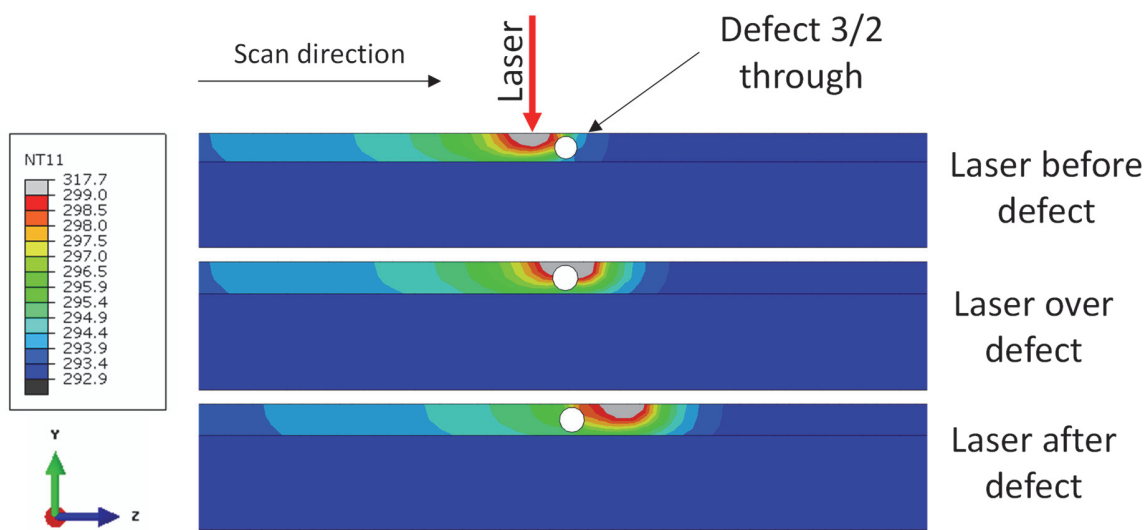


Figure 6: Temperature maps through-the-thickness of the sample 2 with the laser before, over and after the defect zone; temperature scale in Kelvin degree.

Fig. 6 in particular shows the effect of the subsurface hole defects acting as local thermal barriers against heat flow. This determines a temporary surface redistribution of the trail temperature. Such temperature variation suggests that field parameters such as the Mean or the Standard Deviation calculated in a ROI following the laser spot at a short distance, should be sensitive and affected by the presence of defects of any kind.

In Fig. 7 the size and position of five ROIs evaluated in this simulation are presented. ROI 1 is the largest one and includes the other four. ROI 5 is the smallest and the closest to the heat source.

Fig. 8 reports plots of the mean temperature values computed on the five ROIs over the face C of the sample. As can be noticed all five curves deviate from their undisturbed trend each time the heat source flies over a defect, generating a local peak. For this reason the detection of such a local peaks, can be regarded as a defect signature.

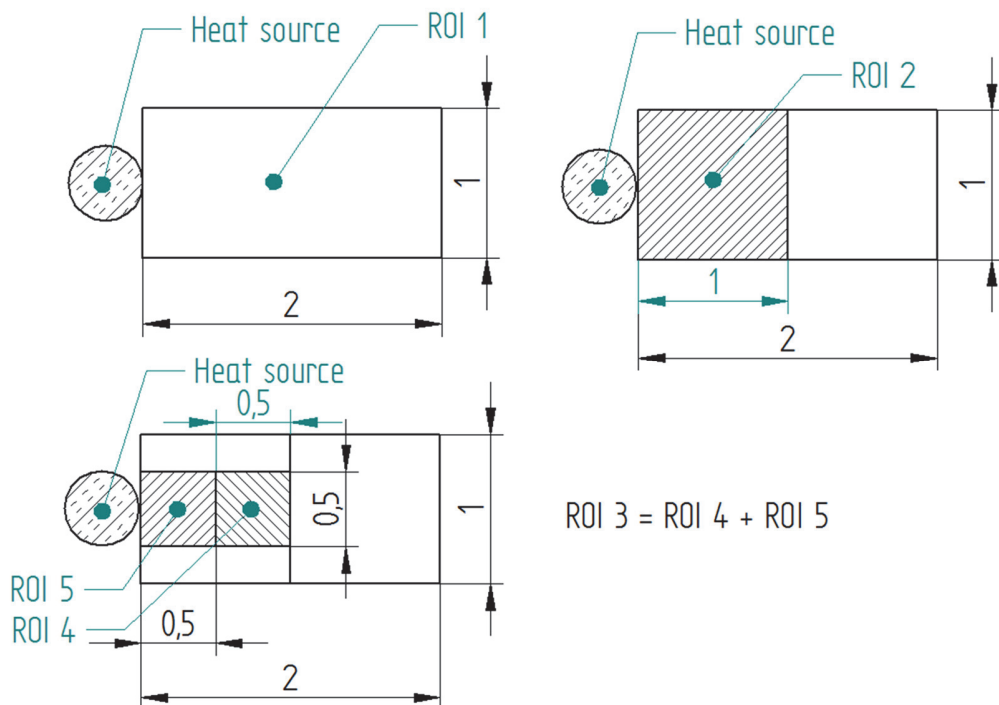


Figure 7: Geometry definition of five ROIs, respect to the heat source used for the defect signature evaluation.

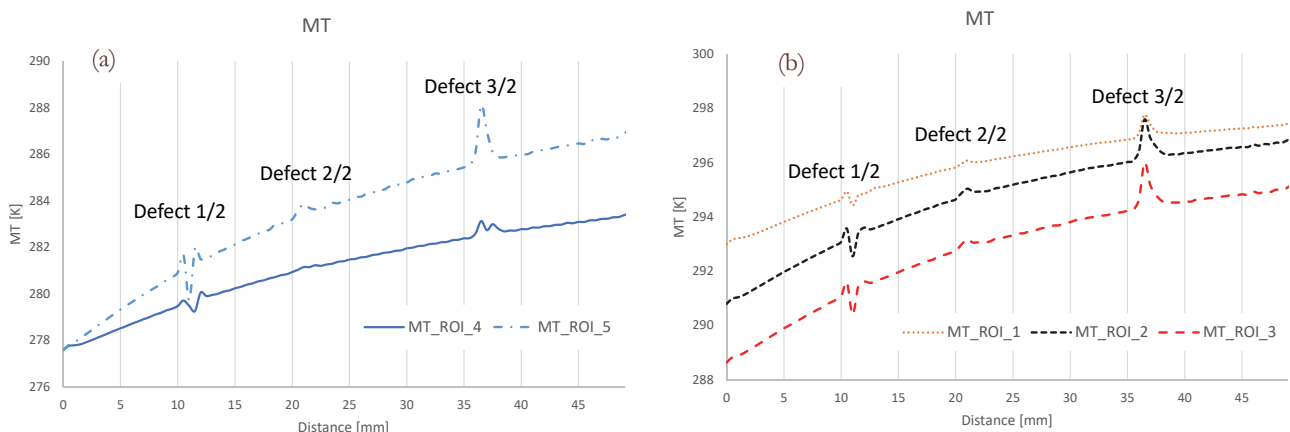


Figure 8: Plots of MT values computed over the five ROI versus the ROI position along face C on sample 2; in (a) ROI 4 and 5, in (b) ROI 1, 2 and 3.

From the results of this simulation, it is first observed that the ideal position of the ROI is the nearest possible to the laser spot (see Fig. 6), on the side of the laser trail (i.e. behind the advancing laser direction), where the temperature field influenced by the defect stretches over a wider area. In order to increase defect sensitivity, the ROI area should be preferably shaped as to include the direction of highest temperature gradients. In this case, as shown by the temperature map of Fig. 6 the temperature highest gradient is located very close to the heat source. This is confirmed by the plot of Fig. 8 where the ROIs that are closer to the heat source present an enhanced peak-to-peak value. In particular, ROI 5, the closest one, seems to be the best choice to enhance defect sensitivity. It is worth noting that the defect signature of the defect 1/2 has a different shape and this is due to the fact that it is superficial and not embedded in the part.

## EXPERIMENTAL RESULTS

Taking into account the results of the FEA, the experiments on the two samples have been performed using a ROI equal to the ones modelled as ROI 5. The chosen ROI for the experiment is a  $0.5 \times 0.5 \text{ mm}^2$  positioned very close to the heat source, where the temperature gradient is the highest. In order to enhance the thermal resolution of the IR camera, the value of the Integration Time set in the present analysis is rather high ( $3000 \mu\text{s}$ ). This choice determines a reduced maximum temperature at which the received radiation saturates the detector. In the present case, the IR camera has such limit at a rather low temperature of about  $40^\circ\text{C}$ . This determines a rather wide zone around the laser spot where the thermal signal is saturated, and then useless for the analysis. Hence, the choice of the best integration time is a trade-off between the need to obtain a high thermal resolution, and the possibility to place the ROI as close as possible to the laser spot.

In Fig. 9 is shown an acquired thermogram where the picked ROI is defined.

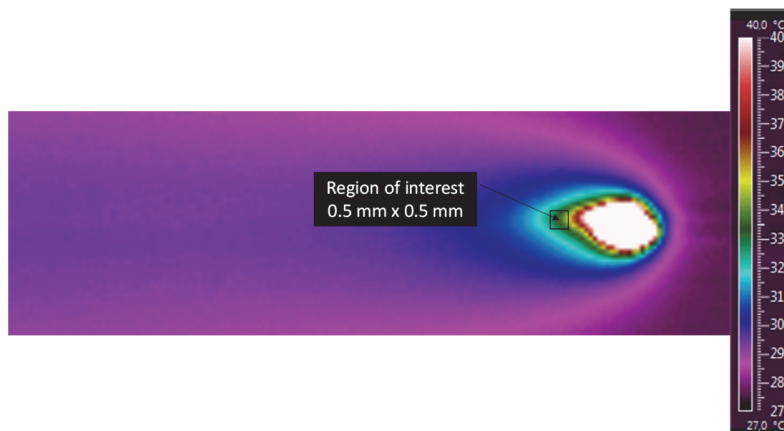


Figure 9: Thermogram acquired on sample 2 with characterization of the region of interest.

Figs. 10a and 10b present the plot of the MT values computed over the ROI versus the ROI position along face A and face B, respectively, on sample 1. As shown in Fig. 10, the four defects of sample 1 are correctly identified. In this case, the FLIPT technique is only able to detect the position of the defect but not its extension, that is overestimated.

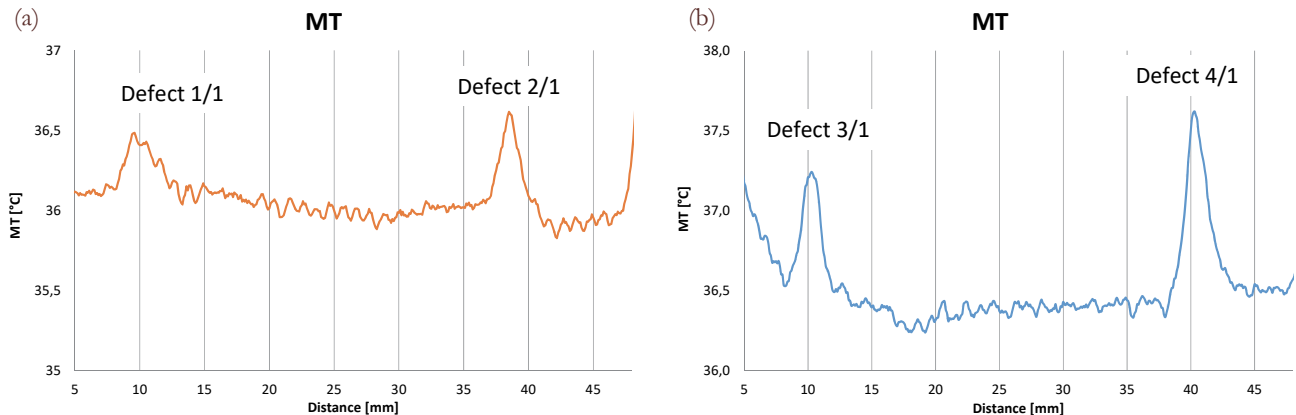


Figure 10: Plots of MT values computed over the ROI versus the ROI position along face A (a) and face B (b) on sample 1.

Fig. 11 shows the plot of MT and SD values computed over the ROI versus the ROI position along face C of sample 2. The perturbations on the MT and SD value along the scanline over the sample 2 allow to spot the three defects correctly. Even in this case, the FLIPT technique is only able to detect the position of the defects but not their extension, that is overestimated. In particular, it is observed that the abscissa corresponding to the defect initiation is well correlated with the initiation of the defect signature. Therefore, the technique is more effective in detecting the beginning of the defect, but less effective in establishing its extension. This is due to thermal inertia effects which remain in the temperature distribution of the ROI which do not allow a clear identification of the instant when the laser spot overcomes the defected zone.

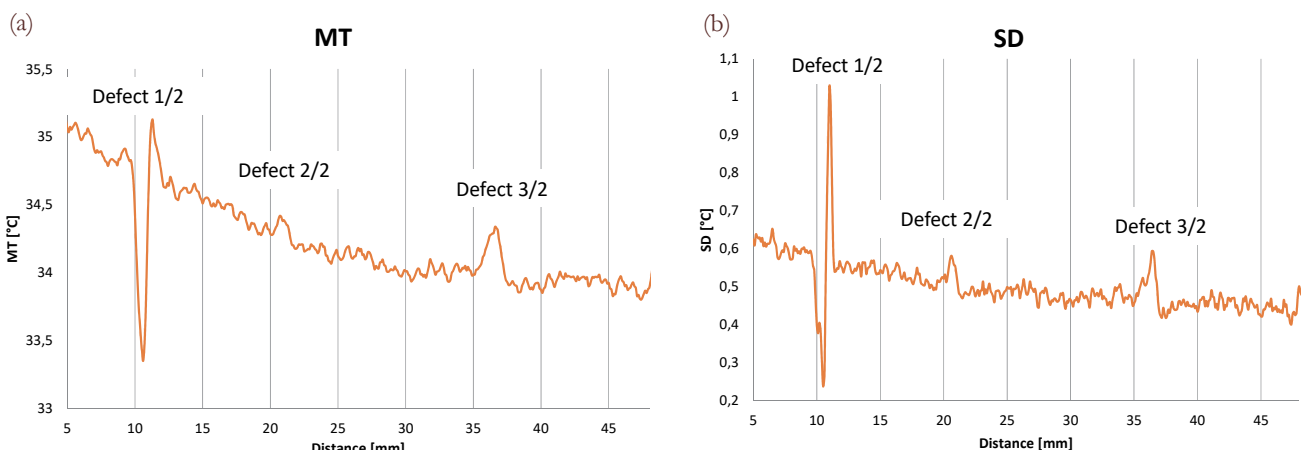


Figure 11: Plot of MT (a) and SD (b) value computed over the ROI versus the ROI position along face C on the sample 2.

#### *Experimental/Numerical Comparison*

In Fig. 12 the MT curves referred to the experimental and numerical outcomes for the scan of face C on sample 2 are compared.

One noteworthy outcome from the above comparison is that both peaks and valleys are well aligned and the relative distances between peaks and valleys of the three defects are similar. In general, the trend of the defect signature is similar between experimental and numerical predictions. The peak-to-peak amplitude is significantly different (the left scale in Fig. 12 refers to the experimental results, while the right scale to the numerical) and is higher for the numerical case, especially for the defect 2/2 and 3/2.

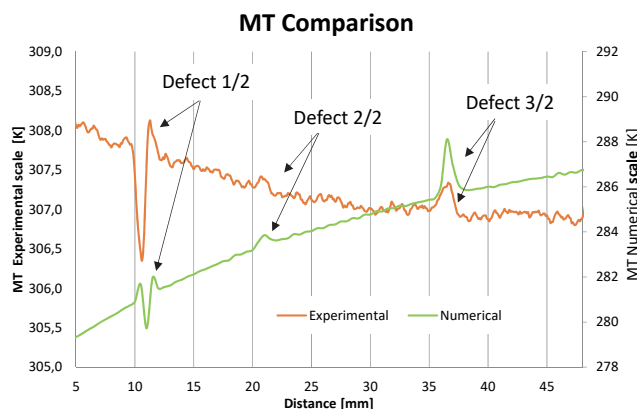


Figure 12: Experimental/numerical comparison of the Mean temperature plot results for the sample 2.

Furthermore, the experimentally detected MT decreases along the laser trajectory, contrary to the numerical prediction. This is due to the different initial thermal conditions of the sample which tend to accumulate the heat from different successive scanning. It is though pointed out that even if the general trends are different, both numerical and experimental curves are able to identify the defects in a very similar manner, and this is considered as a sign of robustness of the proposed approach.

## CONCLUSIONS

**A**dditive manufacturing allows to create 3D complex geometries whose inspection is a big challenge for non-destructive testing methods. The present work demonstrates suitability of a recently proposed laser thermography technique, called “Flying Laser Inner Probing Thermography”, for the on-line detection of typical micro flaws in additive manufactured components. A FEA has been employed to first demonstrate and understand the mechanism of detection in AM components. The same model has been used to adequately tune the parameters of the technique to enhance defect sensitivity. The outcome of the numerical analysis has also been used to identify the optimum size of the ROI to be used for the processing of experimental thermograms. Numerical and experimental results indicate how the technique is able to generate signatures in both tested samples. In particular, this work has demonstrated the advantage of employing a numerical simulation as an aid toward an optimized tuning of experimental parameters. One benefit of the laser thermography as compared to other NDTs is the easy, fast, non-contact, full-field set-up. Some drawbacks may be represented by the need to prepare the surface by applying a matt paint, the difficulty to obtain accurate defect extension evaluations, and the need to use high thermal resolution IR detectors. The remote inspection system by optical methods could potentially be linked to the additive manufacturing rig, in order to achieve monitoring of the entire additive process. The inspection should be performed after layer deposition, when the part has reached room temperature since the equipment cannot stand the heat generated by the process. The technique allows a non-contact and remote inspection showing a potential for in-line automated inspection and processing.

## REFERENCES

- [1] Lewis, G. K., Schlienger, E., Practical considerations and capabilities for laser assisted direct metal deposition, Mater. Des., 21 (2000) 417-423. DOI: 10.1016/S0261-3069(99)00078-3.
- [2] Ahsan, M. N., Bradley, R., Pinkerton, A. J., Microcomputed Tomography Analysis of Intralayer Porosity Generation in Laser Direct Metal Deposition and its Causes, J. Laser Appl., 23 (2011) 022009. DOI: 10.2351/1.3582311.
- [3] Thompson, A., Maskery, I., Leach, R. K., X-ray computed tomography for additive manufacturing: a review, Meas. Sci. Technol., 27 (2016) 072001. DOI: 10.1088/0957-0233/27/7/072001.
- [4] Nilsson, P., Appelgren, A., Henrikson, P., Runnemalm, A., Automatic ultrasonic testing for metal deposition, Proc. 18th World Conference on Nondestructive Testing, Durban, South Africa (2012).



- [5] Nemeth, J., Klien, M., Sears, J. W., Development of Laser Ultrasonics for Defect Detection during Laser Powder Deposition, Proc. TMS Annual Meeting & Exhibition, San Francisco, CA (2005).
- [6] Clark, D., Sharples, S. D., Wright, D. C., Development of Online Inspection for Additive Manufacturing Products, *Insight*, 53(11) (2011) 610-614. DOI: 10.1784/insi.2011.53.11.610.
- [7] Kromine, A. K., Fomitchov, P. A., Krishnaswamy, S., Achenbach, J. D., Laser Ultrasonic Detection of Surface Breaking Discontinuities: Scanning Laser Source Technique, *Mater. Evaluation*, 58 (2) (2000) 173-177.
- [8] Klein, M., Sears, J., Laser ultrasonic inspection of laser cladded 316LSS and Ti 6-4, Proc. 23rd Int. Congress on Applications of Lasers and Electro-Optics, San Francisco, CA (2004).
- [9] Edwards, R. S., Dutton, B., Clough, A. R., Rosli, M. H., Scanning Laser Source and Scanning Laser Detection Techniques for Different Surface Crack Geometries, Review of Progress in Quantitative Nondestructive Evaluation, Proc. AIP Conference, Burlington, VT, (2011) 251-258. DOI: 10.1063/1.4716237.
- [10] Cerniglia, D., Scafidi, M., Pantano, A., Rudlin, J., Inspection of additive-manufactured layered components, *Ultrasonics*, 62 (2015) 292-298. DOI: 10.1016/j.ultras.2015.06.001.
- [11] Li, T., Almond, D. P., Rees, D. A. S., Crack imaging by scanning laser-line thermography and laser-spot thermography, *Measurement Science and Technology*, 22(3) (2011) 035701.
- [12] Burrows, S. E., Rashed, A., Almond, D.P., Dixon, S., Combined laser spot imaging thermography and ultrasonic measurements for crack detection, *Nondestructive Testing and Evaluation*, 22 (2007) 217-227. DOI: 10.1080/10589750701448605.
- [13] Montinaro, N., Cerniglia, D., Pitarresi, G., Detection and characterization of disbonds on fibre metal laminate hybrid composites by flying laser spot thermography, *Composites Part B: Engineering*, 108 (2017) 164-173. DOI: 10.1016/j.compositesb.2016.09.084.
- [14] Burrows, S. E., Dixon S., Pickering S. G., Li T., Almond D. P., Thermographic detection of surface breaking defects using a scanning laser source, *NDT&E International*, 44 (2011) 589-596. DOI: 10.1016/j.ndteint.2011.06.001
- [15] Schlichting J., Maierhofer C.h., Kreutzbruck M., Crack sizing by laser excited thermography, *NDT&E International*, 45 (2012) 133-140. DOI: 10.1016/j.ndteint.2011.09.014.
- [16] Montinaro, N., Cerniglia, D., Pitarresi, G., Flying laser spot thermography technique for the NDE of fibre metal laminates disbonds, *Composite Structures*, 171 (2017) 63-76. DOI: 10.1016/j.compstruct.2017.03.035.